Korean J. Chem. Eng., 38(9), 1934-1945 (2021)
DOI: 10.1007/s11814-021-0838-9

pISSN: 0256-1115
eISSN: 1975-7220

Recovery of Tin as Tin oxide nanoparticles from waste printed circuit boards for photocatalytic dye degradation

Dina Magdy Abdo*, Sabah Mohamed Abdelbasir*,†, Shakinaz Taha El-Sheltawy, and Ibrahim Ahmed Ibrahim***

*Central Metallurgical Research and Development Institute, P.O. Box: 87, Helwan, 11421, Cairo, Egypt
**Faculty of Engineering, Cairo University, Giza, Egypt
(*Received 16 February 2021 • Revised 1 May 2021 • Accepted 4 May 2021*)

Abstract−A simple eco-friendly process is proposed to retrieve tin from waste printed circuit boards (WPCBs) as tin oxide nanostructured powders. The WPCBs were leached in disodium salt of ethylene diamine tetraacetic acid (Na_2-EDTA) chelating agent comparing results with acid leaching. Parameters affecting the leaching process such as sample particle size, pH, temperature, time, liquid/solid ratio, and concentration of Na_2-EDTA were investigated. A 100% of Sn can be recovered by leaching in 0.1 mol/L Na_2-EDTA solution for 3 hours at 80 °C with optimum conditions of pH: 5, liquid/solid ratio: 30, particle size −0.07 mm, and constant stirring of 400 rpm. Kinetic data suggest a diffusion-controlled process as the rate-determining step for the Na_2-EDTA extraction of tin from WPCBs with an activation energy of 15.28 KJ·mol^{-1}. Selective precipitation of Sn as tin oxide (SnO_2) nanoparticles (NPs) from leachant solution was performed via a simple route using sodium hydroxide. Characterization tests (XRD, FTIR, EDX, FE-SEM, and TEM) were made to confirm the morphology of the nanoparticles. The prepared SnO_2 NPs, having a size range of 8-12 nm, showed an excellent photocatalytic action towards methylene blue (MB) dye under ultraviolet (UV) light illumination with 90% efficiency after 180 min and showed good reusability after five consecutive cycles.

Keywords: Waste Printed Circuit Boards, Tin Recovery, Leaching, Chelating Agent, Kinetics, SnO_2 Nanoparticles, Dye Degradation

INTRODUCTION

A crucial constituent of all electronic waste (e-waste) is the printed circuit board (PCBs) that contains various sorts of metals and non-metals [1]. WPCBs characteristically consist of metallic, plastic, and ceramic materials with variable composition contingent on their particular classification [2]. There are many metallic components, for example, Cu, Sn, Pb, Zn, Ni, and Fe just as some valuable metals like Ag, Pd, and Au [3]. Tin alloys are specifically utilized for the binding of different electronic components to the PCBs because of their satisfactory mechanical features and low temperature of melting [4]. Thus, Waste PCBs can be viewed as important, valued metal resource and need to be recycled properly. The dangerous components in WPCBs pose a real threat to human wellbeing and feasible monetary development also. WPCBs comprise various toxic heavy metals, such as lead, cadmium, arsenic, antimony, beryllium, chromium, and mercury in addition to plastics with brominated flame retardants and polyvinyl chloride [5]. When exposed for resource recovery or subjected to a procedure, these elements get liberated into the environment, exceeding the permissible limit, and become a potential threat to human health and the environment.

During PCBs fabrication, a tin weld is plated onto the copper surface for etching resistance, and electronic components (chips, resistors, capacitors, etc) are mounted onto the PCBs with tin solder [6]. Desoldering and detaching electronic components (ECs) has to be the first step to recover valued metals from WPCBs [7].

Looking at the advantages of recycling, expanding consideration has been paid to the development of recycling techniques for yielding metal values from various types of e-waste. The recycling approaches mostly follow the physical pre-treatment with ensuing pyro- and/or hydro-metallurgical operations [8]. Hydrometallurgical practices offer an ecological and facile technique of metal separation from various plastics and ceramic materials [9]. Recently, the development of hydrometallurgical routes for WPCBs recycling has been intensely highlighted [10-12]. A significant number of researches concentrated on copper [13-15] and precious metals' recovery [16] have been reported. Yet, tin and lead present in solder alloy considerably complicate their leachability for recovery [17]. Treatments via bioleaching [18], alkaline [19], nitric [20], hydrochloric [21,22], or fluoroboric acid [23] as leachants are described.

Tin recovery methods are extremely contingent on the amount in solution. For dilute solutions, various removal methods including solvent extraction, cementation, and ion exchange are present [24,25]. In PCBs, metals are epitomized with plastics and ceramic causing many problems in powerful leaching; thus, it is very important to separate metallic and polymeric constituents [26]. Tin leaching from the debilitated PCBs using hydrochloric acid is improved after removing the varnish that led to the increase in reaction interface [27]. $SnCl_4$ and HCl were also considered to successfully leach and recover Sn, along with Ag and Cu from solder [28]. Recently, indium and tin were separated and recovered from spent indium-tin oxide (ITO) targets by leaching in concentrated HCl. After distillation, the obtained indium and tin ions crystals were

†To whom correspondence should be addressed.
E-mail: sfoda20@hotmail.com
Copyright by The Korean Institute of Chemical Engineers.

transferred into $SOCl_2$ solution under refluxing, and by fractionating the mixture, anhydrous indium chloride, tin tetrachloride, and $SOCl_2$ were separated with recovery rates of 99.6% and 98.0% for $InCl_3$ and $SnCl_4$ and purity higher than 99.0% [29].

Nitric acid was also used for tin leaching from WPCBs [30]; however, the main drawback of this process is nitrogen oxide emissions.

Tin oxide (SnO_2) is one of the most significant materials [31], having a high degree of transparency in the visible range, strong interaction with adsorbed species, low performing temperature, and strong stability at high temperature (~500 °C) [32]. It is also an n-type semiconductor with a high bandgap (3.6 eV) [32]. According to the literature, SnO_2 nanoparticles are produced by various methods such as hydrothermal [33], sonochemical [34], mechanochemical [35], thermal decomposition [36], evaporation of powdered oxides [36,37], sol-gel [38], and co-precipitation [39]. Tin oxide (SnO_2) is one of the most investigated transparent conducting oxides (TCOs), mainly due to its high optical transparency in the visible region, high electrical conductivity, and wide band-gap [40]. It is a promising candidate for optoelectronic applications such as solar cells, photocatalysis, photo transistors, gas sensors, batteries, transistors, and transparent electrodes [41,42]. On the other hand, SnO_2 offers a potential role in short-wavelength light-emitting diodes (LEDs) due to its higher exciton binding energy of 130 meV and wider band gap at room temperature compared with GaN [43]. It also offers high sensitivity and rapid response to many gases, and doping with suitable dopants is demonstrated to be among the most effective approaches for boosting its selectivity to particular gases [44].

On the other hand, dyes are looked to as one of the foremost pollutants to create an environmental threat to the aquatic system. Numerous investigations have been done to remove organic dyes from effluents [45-47]. Their stable complex structure makes them difficult to eliminate from effluents. Photocatalytic degradation with the help of nanomaterials can provide effective elimination of these toxic pollutants from the environment [48]. SnO_2 nanoparticles can attach to the noxious chemicals' surface, because of their ultrasmall size, causing their degradation [49]. Though SnO_2 has been applied as a constituent of composite with TiO_2 and ZnO as photocatalysts [50], and its use as the pure form is rarely reported possibly due to the problematic formation of mixed phases of SnO or Sn^0 that could exist in the catalyst [50].

This study aims to recycle WPCBs for their metallic content and recover from this toxic material value-added tin oxide (SnO_2) nanoparticles via selective leaching in Na_2-EDTA chelating agent and compare with usual acid leaching. Various parameters such as leachant concentration, time, temperature, and solid/liquid ratio were considered. SnO_2 nanoparticles were precipitated from leachant solution using the simple and inexpensive route. Finally, the photocatalytic property of the nanoparticles to break down methylene blue (MB) dye under UV irradiation was investigated.

EXPERIMENTAL WORK

1. Materials and Chemicals

A sample of mechanically processed waste printed circuit boards (PCBs) weighing 6 Kg was provided by the International Technological Group Company (ITG), a privately authorized e-waste recycling group, Cairo. It was ground using a disc mill (Retsch, Germany) to - 3.0 mm. A scanning electron microscope (SEM) and the energy-dispersive X-ray spectroscopy (EDX) analysis of the WPCBs sample are shown in Fig. 1. From the figure, we can see that the WPCBs powder is irregular and contains many-valued elements (for instance Cu, Pb, Sn, Al, Zn, and Si). The EDX analysis confirmed the existence of these elements either in the elementary form or alloys as reported earlier by Ha and his coworkers [51]. Ethylene diamine tetraacetic acid disodium salt (Na_2-EDTA) and sodium hydroxide (NaOH) were obtained from Sigma-Aldrich and used as received with no further treatment. Extremely purified water was used in all work.

2. Leaching Practice

Table 1 displays the chemical composition of the WPCBs sample estimated by X-ray fluorescence spectrometry (XRF), and a photo of the WPCBs before and after grinding is displayed in Fig. S1 in the supplemental file. According to the table and loss-on-

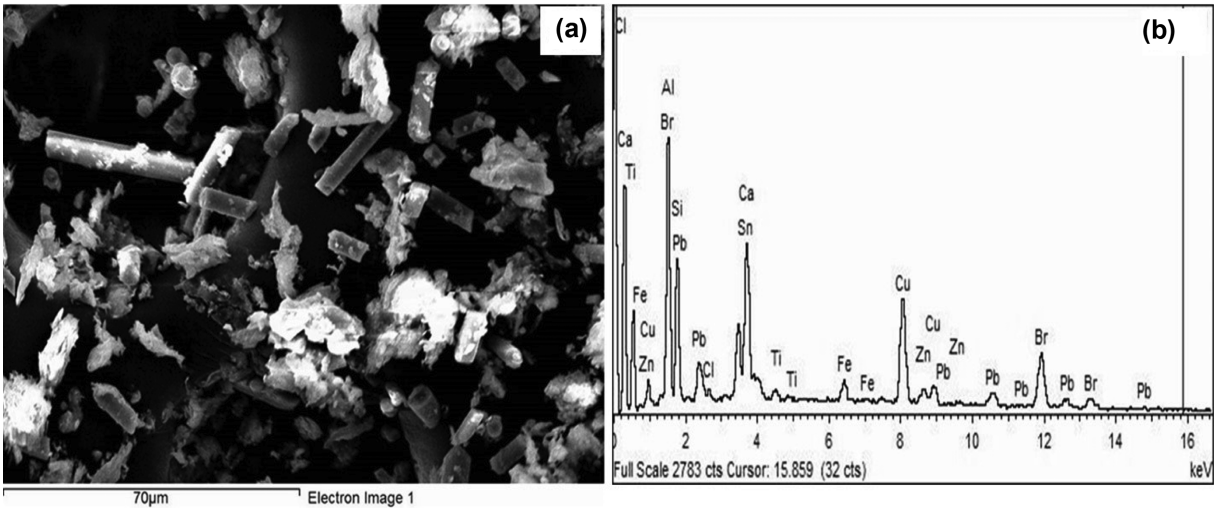


Fig. 1. SEM image (a) and EDX spectra (b) of WPCBs sample.

Table 1. Chemical composition of the WPCBs sample determined by XRF

Element	Cu	Zn	Sn	Fe	Pb	Sb	Ni	Br	Ba	Si	Sr	Mg	Ca	Al
Content (wt%)	21.96	2.62	16.15	2.32	8.40	2.67	0.47	21.96	1.41	0.35	0.14	0.10	0.50	0.16

ignition data, the composition of the studied WPCBs is constituted by approximately 52 wt% metals.

Leaching was accomplished in a 1-L three-necked Pyrex reactor. This reactor was set in a water bath placed above a magnetic stirring hotplate. A reflux condenser was attached through the central opening of the glass reactor lid to avoid acid evaporation at higher temperature. The second neck was used for inserting a pH electrode probe and the third neck was used for sampling. First, the leaching solutions were put into the reactor, then a certain amount of waste PCBs powders was added and this was marked as the launch of the experiment. Experiments were implemented to study the effect of the leachant concentration on tin extraction at a temperature range of 50 °C-90 °C using constant agitation speed (400 rpm) for different periods ranging from 30-240 min. The liquid to solid ratio (L/S ratio) was varied between 20-40. The system used is represented in Fig. S2 in the supplemental file. After the leaching experiments were ended, solutions were separated from the solid residues by filtration and the extent of tin extracted was determined by (ICP). Leaching experiments and analysis were performed in triplicate for accuracy.

The percentage of tin metal recovery was determined as shown in Eq. (1)

$$\text{Tin extraction (\%)} = \frac{\text{Tin extracted into the leaching solution} \times 100}{\text{Total tin in the WPCBs sample}} \quad (1)$$

3. Fabrication of the Nanoparticles

SnO_2 was produced from the leachant solution as nanoparticles via the coprecipitation method. Leach liquor of WPCBs sample obtained at optimized condition (0.1 mol/L Na_2-EDTA) was treated by NaOH solution to precipitate tin oxide nanoparticles at pH 9.0 and temperature of 60 °C. The nanoparticles were separated by centrifugation, cleansed repeatedly using extra pure water and alcohol then, annealed at 500 °C in a muffle furnace (Nabertherm LT, Germany) for two hours.

4. Characterization Tests

The waste PCBs powder sample was analyzed by X-Ray Fluorescence (XRF, Axios Advanced WDXRFP analytical, Netherland). Samples taken at different time durations during experiments were analyzed using ICP-OES, Optima 2000 DV spectrometer. The phase identification was analyzed with an X-ray diffractometer (Bruker AXS-D8, Germany, Cu-Kα λ=1.5406 Å at 2θ from 20 to 70°. Both transmission (TEM, JEOL-JEM-1230, Japan) and field emission scanning electron microscope (FE-SEM; QUANTAFEG 250, Netherlands) were used for structural investigation of the nanoparticles. FTIR spectra of the produced samples were verified by a JASCO 3600 spectrometer. XPS spectra were recorded using a K-ALPHA photoelectron spectrometer (Thermo Fisher Scientific, USA) with 10-1,350 eV radiation spot size 400 μm at pressure 10^{-9} mbar.

5. Evaluation of Photocatalytic Properties

Photocatalytic action of the SnO_2 NPs was evaluated by the degradation of MB at different times (0-300 min) UV using Luzchem LZC 4V (Canada) multi-lamp photoreactor at a wavelength of 350 nm under regular stirring. Experimentations were achieved on MB dye solutions (10 ppm, 18 mL) using 0.1 g of the nanoparticles. The pH value of the initial MB solution was adjusted to be in the range of 5.5-6 with 0.1 M HCl or NaOH solution. Solutions were first stirred in dark for 30 min to accomplish equilibrium, then irradiated for the defined time of the experiment. Samples were analyzed at 665 nm of MB dye using a UV-vis spectrophotometer (Varian Cary 100). After complete dye decolorization, the catalyst was centrifuged and reused five times to check the stability and reusability of the catalyst. After each cycle, the SnO_2 nanoparticles were separated from the reaction mixture by centrifugation at 4,000 rpm for 10 min, washed many times with ultrapure water and dried at room temperature. In the next cycle, the SnO_2 nanoparticles were reused for the degradation of fresh dye solution. The degradation percentage of MB was calculated using the following relation:

$$\text{Degradation \%} = \frac{C_o - C_t}{C_o} \times 100 \quad (2)$$

where C_o and C_t are the initial MB dye concentration and the concentration at reaction time t, respectively.

RESULTS AND DISCUSSION

1. Leaching Process

XRD analysis (Fig. 2) was performed to identify the crystalline phases of waste PCBs. Metallic copper, tin, lead, aluminum, and iron were found to be the main phase constituents.

Effect of the leachant concentration (Na_2-EDTA, HNO_3, and H_2SO_4) on the extraction percentage of tin was inspected using 5.0 g of WPCBs powder, leaching time of 3 hours at 80 °C, liquid

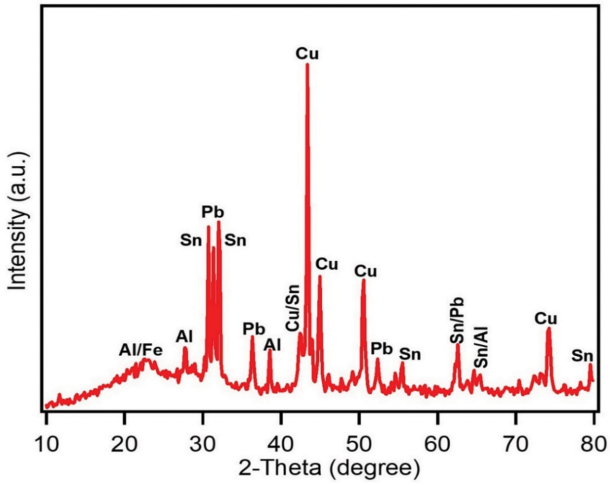


Fig. 2. XRD pattern of the powdered WPCBs.

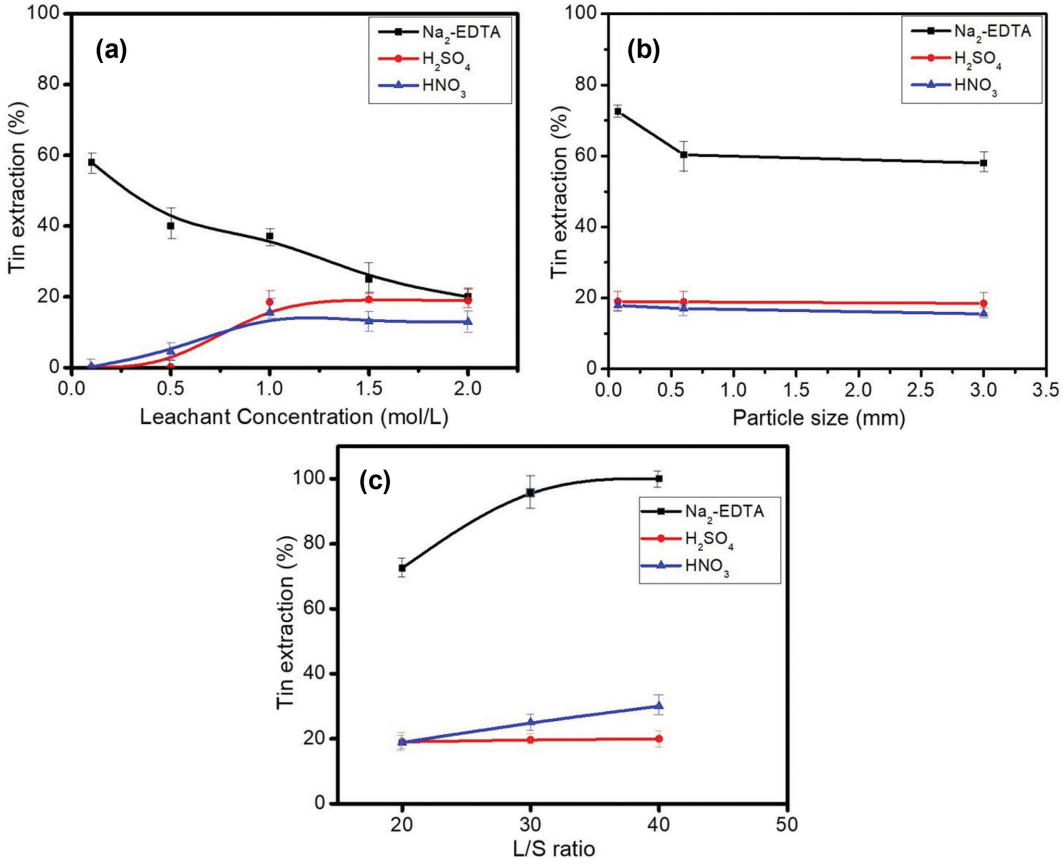


Fig. 3. Effect of: (a) Leachant concentration, (b) particle size, (c) on the extraction percentage of tin from WPCBs (leaching conditions: time: 3 hours; leachant concentration: 1 mol/L; particle size: −0.07 mm; rpm: 400 and temperature: 80 °C).

to solid (L/S) ratio of 20, and constant stirring of 400 rpm. Acid and Na_2-EDTA concentrations were varied from 0.1 mol/L to 2.0 mol/L. Results in Fig. 3(a) show that increasing Na_2-EDTA concentration had an undesirable impact on the extraction of tin metal. When the concentration was increased from 0.1 mol/L to 2.0 mol/L, the extraction of Sn decreased from 60.0% to 20.0%, whereas it increased from 1.0% and 5.0% to 12.0% and 17.0% in the case of HNO_3 and H_2SO_4 acids, respectively. Not more than 20% of Sn extraction was achieved using sulfuric and nitric acids as leachants. Usually, the kinetics of tin leaching in dilute sulfuric acid is very slow and requires long periods. Tin extraction would likely require a very strong acid. During nitric acid leaching, tin precipitates as stannic acid ($SnO_2 \cdot H_2O$) [52], according to the following reactions:

$$3Sn+4HNO_3+H_2O \rightarrow 3SnO_2 \cdot H_2O+4NO \quad (3)$$

$$Sn+4HNO_3 \rightarrow SnO_2 \cdot H_2O+4NO_2+H_2O \quad (4)$$

The considerably high leaching temperature accelerates the precipitation of tin as tin hydroxide. On the other hand, some references specify that SnO_2 and SnO, with amphoteric property, are soluble in strong acids or alkalis. Particularly, reactions between Sn^{2+} and Sn^{4+} oxides with H_2SO_4 forming sulfates ($Sn(SO_4)_2$ and $Sn(SO_4)$. Once formed, $Sn(SO_4)$ remains in H_2SO_4 solution, but $Sn(SO_4)_2$ precipitates as $Sn(SO_4)_2 \cdot 2H_2O$ [53] as follows:

$$SnO_2+2\ H_2SO_4 \rightarrow Sn(SO_4)_2+2H_2O \quad (5)$$

$$SnO+H_2SO_4 \rightarrow Sn(SO_4)+H_2O \quad (6)$$

In the case of Na_2-EDTA leaching, tin forms a complex which precipitates as hydroxide upon excess addition of NaOH as follows:

$$Sn^{2+}+Na_2\text{-EDTA} \rightleftharpoons Sn_2\text{-EDTA} \quad (7)$$

$$Sn_2\text{-EDTA}+NaOH \rightarrow Na_2\text{-EDTA}+Sn(OH)_2 \quad (8)$$

When calcined at 500 °C, dehydration followed by oxidation reaction occurs and SnO_2 nanoparticles are produced [54] as follows:

$$Sn(OH)_2 \rightarrow SnO+H_2O \quad (9)$$

$$SnO+O_2 \rightarrow SnO_2 \quad (10)$$

Metal leaching was additionally investigated in accord with the WPCBs particle size using 5.0 g of WPCBs powders with L/S ratio of 20 at 80 °C and a constant stirring speed of 400 rpm. The outcomes are presented in Fig. 3(b), from which it can be seen that the particle size of WPCBs powder negatively affects the Sn metal extraction by EDTA from 73% to 60% for −0.07 mm and 0.5 mm, respectively, but had no effect when either sulfuric or nitric acid was used for leaching. In the case of reduced particle size, the interaction extent between particles and leachant improved leading to higher dissolution and hence higher extraction.

Fig. 3(c) demonstrates the effect of L/S ratio on tin extraction percent. L/S ratio (ml/g) was increased from 10 to 30 keeping the

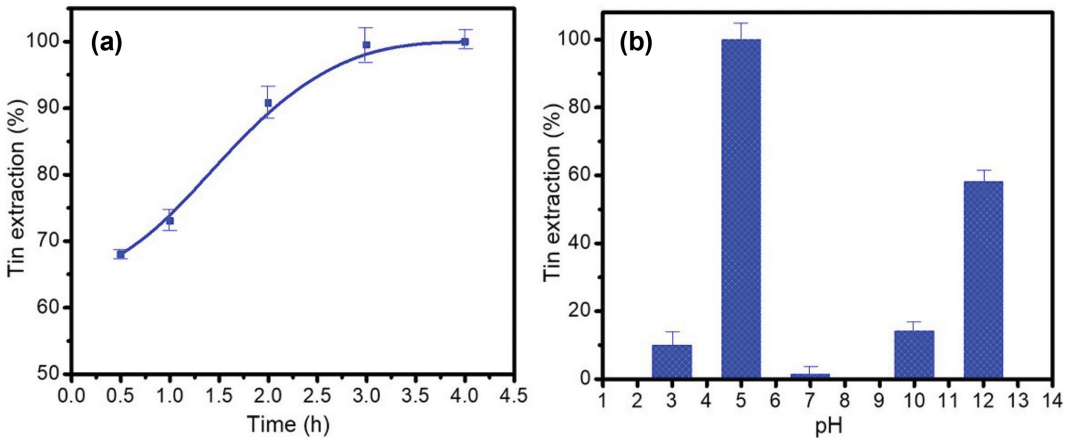


Fig. 4. Effect of: (a) Leaching time, (b) pH on the extraction percentage of tin from WPCBs using 0.1 mol/L Na_2-EDTA for particle size: −0.07 mm; leaching time: 3 hours; pH: 5; L/S ratio: 30; rpm: 400 and temperature: 80 °C.

leachant concentration constant (0.1 mol/L of Na_2-EDTA and 1.0 mol/L for both H_2SO_4 and HNO_3 acids). Almost a 26% increase in tin extraction % occurred when the L/S ratio increased from 20 to 30 to reach 99.55% extraction. No considerable change in the extraction efficacy was ascertained with the upsurge in L/S ratio in the case of H_2SO_4 acid leaching, while it increased from 20% to 29% in the case of leaching with HNO_3. This can be explained by the fact that the reactant is present in the solution in greater amounts than required for leaching reaction and, hence, fluctuation in L/S ratio has no significant effect on the extraction process [55].

The effect of reaction time on extraction efficiency was studied at pH: 5 for periods from 0.5 hours to 4 hours, results are in Fig. 4(a). We can notice that the amount of tin extracted increases with time to reach a maximum value of 99.55% at 3 hours leaching, which was, therefore, deemed as the optimum leaching time for extracting Sn from WPCBs when compared to other two leachants (HNO_3 and H_2SO_4) at the same leaching conditions (as revealed in Fig. 5).

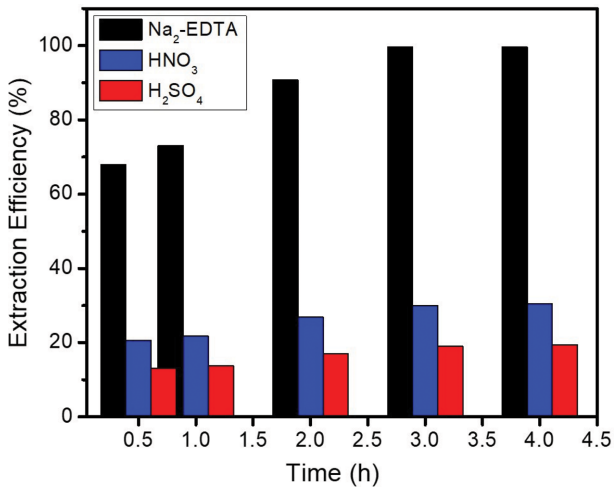


Fig. 5. Extraction efficiency of tin from WPCBs using 0.1 mol/L of the three leachants (particle size: −0.07 mm; leaching time: 3 hours; pH: 5; L/S ratio: 30; rpm: 400 and temperature: 80 °C).

To examine the effect of pH on Sn extraction from WPCBs, leaching experiments were performed at pH ranging from 3 to 12, results are in Fig. 4(b). Conditions were as follows: leaching for 3 hours in 0.1 mol/L Na_2-EDTA for −0.07 mm particle size, L/S ratio: 30 at 80 °C, and constant stirring with 400 rpm. As claimed by Chauhan and coworkers [56], the % distribution of various protonation steps strongly affects the pH range for a chelating agent; thus, an improvement in extraction efficiency was gained from 10% to 99.55% with the increase in reaction pH from 3 to 5, then decreases sharply to 3% at pH 7, after that increases with pH rise to 12 reaching 58%. Hence, pH 5 was the optimum pH value considered for the maximum extraction of Sn from WPCBs powder. Solution pH positively controls the chelating agent performance when used for leaching metals [57,58]. pH affects the concentration of metals in the solution, the chelant solubility, and accordingly, the stability of the formed complexes [58,59]. As the H^+ ions increase in the medium, the particle surface becomes more protonated and positively charged; in this way enhancing the sorption of negatively charged metal chelates leading to a higher extraction percentage of metals from the solid PCBs powder [60].

2. Kinetic Study of the Leaching Process

Kinetics of leaching tin from WPCBs powder was examined at a varying concentration of Na_2-EDTA to configure the mechanism of leaching. The data achieved with 0.1 mol/L Na_2-EDTA at a fixed L/S ratio of 30 varying temperatures from 50-90 °C was scrutinized to find out best fitting with known kinetics model equations.

The leaching rate commonly obeys three controlling models: either diffusion through a liquid film, a surface chemical reaction, or diffusion through a product layer. Moreover, the mixed kinetic model equation (reliant on diffusion-controlled mechanisms) can also be applied to set the leaching rate constants. The rate equation of each model is respectively written as:

$$x=k_t t \quad (11)$$

$$1-(1-x)^{1/3}=k_r t \quad (12)$$

$$1-3(1-x)^{2/3}+2(1-x)=k_d t \quad (13)$$

$$[1-(1-x)^{1/3}]^2=k_m t \quad (14)$$

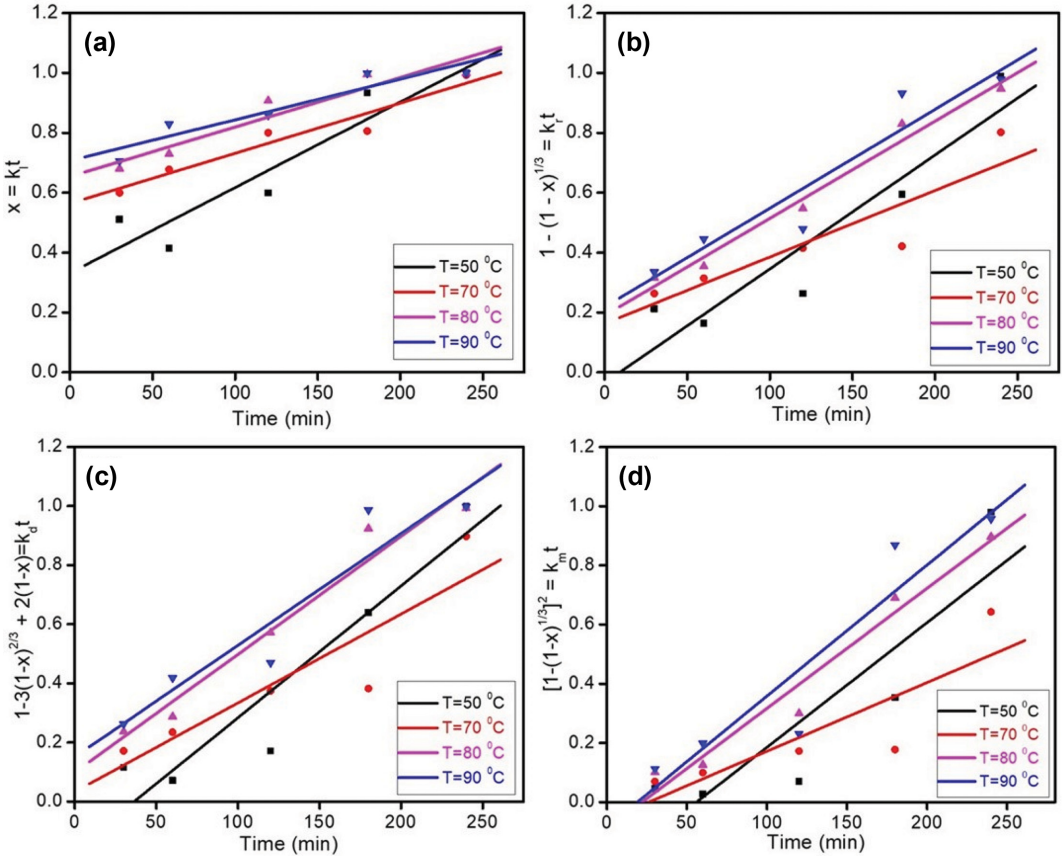


Fig. 6. Plot of different kinetic models for tin leaching in 0.1 mol/L Na_2-EDTA solution (L/S ratio 30; rpm: 400; particle size: −0.07 mm): (a) Diffusion through the liquid film; (b) surface chemical reaction; (c) diffusion through the product layer; (d) mixed kinetic model.

where x and t are the conversion fraction of solid particles and the reaction time. k_1, k_r and k_d are the rate constant for the above models, respectively.

Based on kinetic models in the literature, leaching data were evaluated using Eqs. (11) to (14) to get the rate-monitoring step. Rate constants and correlation coefficients were calculated and revealed in Table S1 in the supplemental file. Plotting of the four relationships between (x), $1-(1-x)^{1/3}$, $1-3(1-x)^{2/3}+2(1-x)$ and $(1-(1-x)^{1/3})^2$ against the time for tin leaching at varied temperatures (Fig. 6(a)-(d) designates a good correlation with the diffusion through the liquid film model. This result is decided on the higher value of regression coefficient (R^2) value for selected equation (0.94, 0.96, 0.95, and 0.96 at 50 °C, 70 °C, 80 °C, and 90 °C correspondingly). Depending on the activation energy (E_a) value, we can decide if the leaching reaction is diffusion or chemical controlled. To figure out the activation energy for tin leaching from WPCBs powder, a plot was also drawn between ln k and 1/T (Arrhenius plot). The calculated activation energy equaled 15.28 KJ mol^{-1} (Fig. 7), confirming that the leaching reaction is under control of diffusion through the liquid film model as it is lower than 20 kJ/mol as reported earlier by many researchers.

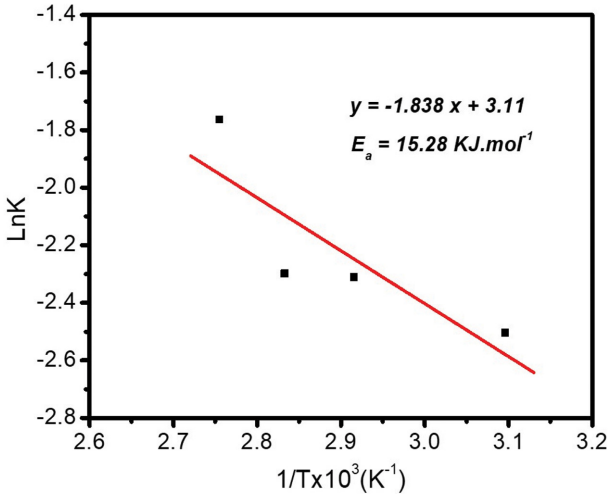


Fig. 7. Arrhenius plot for tin leaching from WPCBs in 0.1 mol/L Na_2-EDTA chelating agent.

3. SnO_2 Nanoparticles Preparation from the Leach Liquor

XRD examination was made to assure the formation of the particles. Results displayed in Fig. 8(a), show that all diffraction peaks at 2θ of 26.60, 33.90, 38, 51.8, 54.8, 61.9°, and 66.90 indicate the formation of SnO_2 nanoparticles. The highest peaks correspond to the (110), (101), and (211) planes of SnO_2 lattice as recognized using JCPDS card no. 72-1147. No peaks of impurities were distinguished, reflecting the purity of the obtained particles. The average SnO_2 crystallite size figured by the Scherrer equation is 10-

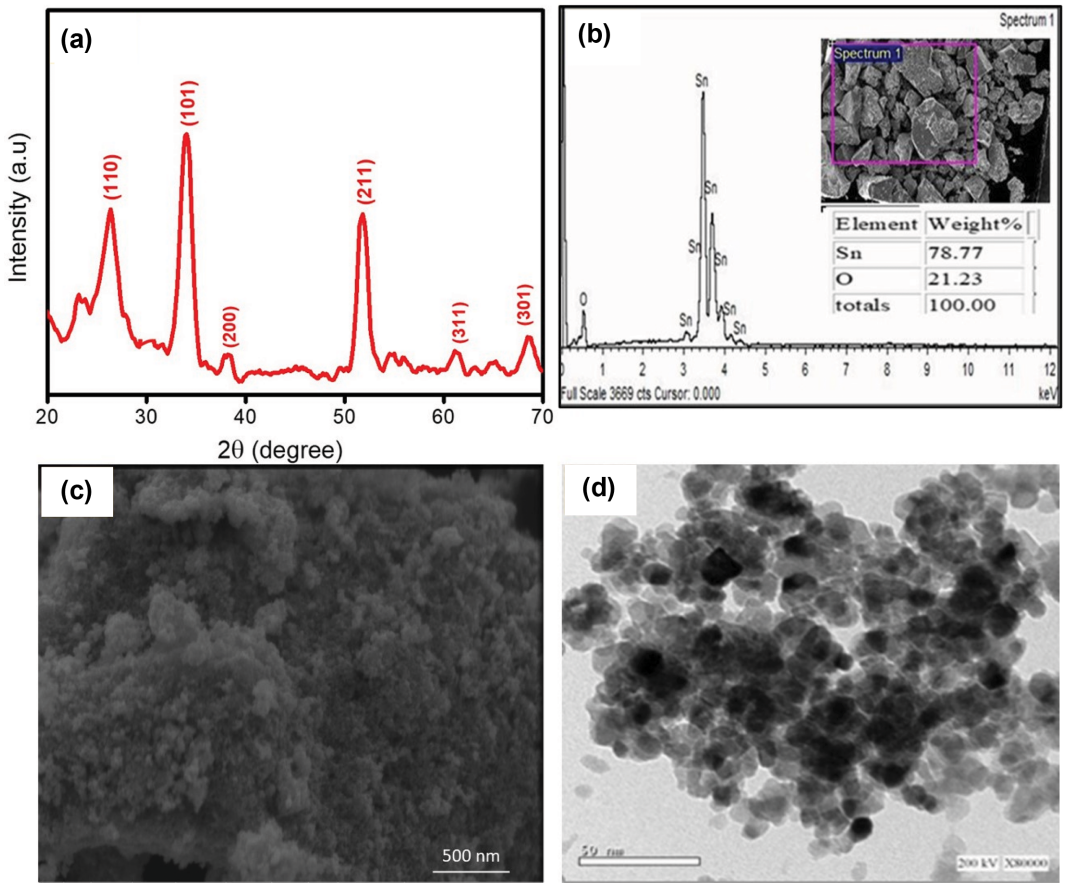


Fig. 8. (a) XRD; (b) EDX; (c) SEM image and (d) TEM image of the as-synthesized SnO_2 nanoparticles.

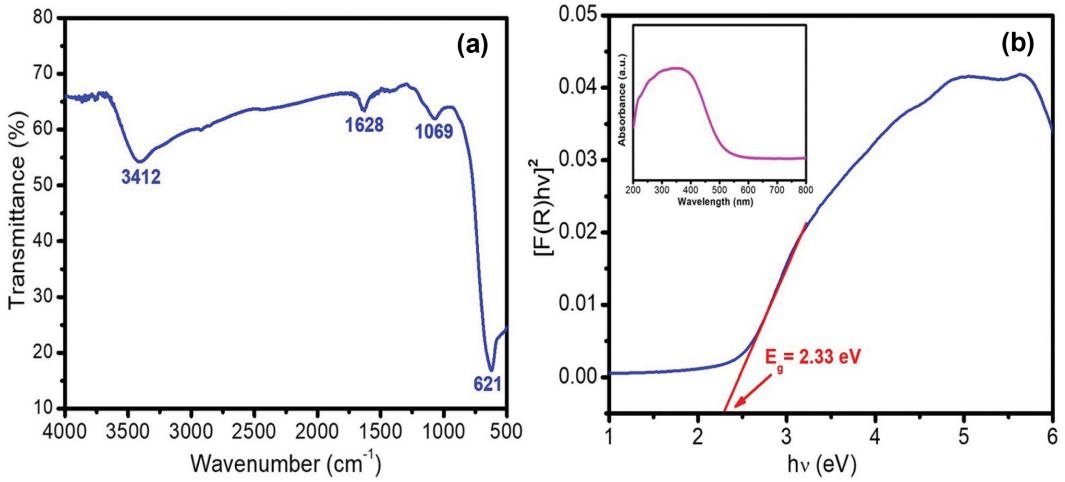


Fig. 9. (a) FTIR spectra; (b) plot of $(\alpha h\nu)^2$ vs phonon energy of SnO_2 nanoparticles (inset Uv-Vis. spectra of SnO_2 nanoparticles).

12 nm. As the particle size decreases to the nanosized, agglomeration predominates [61]. EDX analysis in Fig. 8(b) shows the sample peaks relating to only Sn and O at 3.6, 0.5 eV, respectively, indicating also the purity of SnO_2.

The morphology of the SnO_2 NPs was inspected by FE-SEM. As one can see in Fig. 8(c), samples are composed of polydisperse spheres that are very small and aggregated into larger particles. TEM analysis, giving more info about the morphological structure of SnO_2 NPs, is shown in Fig. 8(d) from which we can see that the prepared SnO_2 NPs are haphazardly clustered spheres of approximately 12 mm size.

Fig. 9(a) shows the FTIR spectra of SnO_2 NPs. The peaks at 3,412 cm^{-1} and 1,628 cm^{-1} are ascribed to O-H stretching vibrations of water or OH groups absorbed at the exterior surface of the

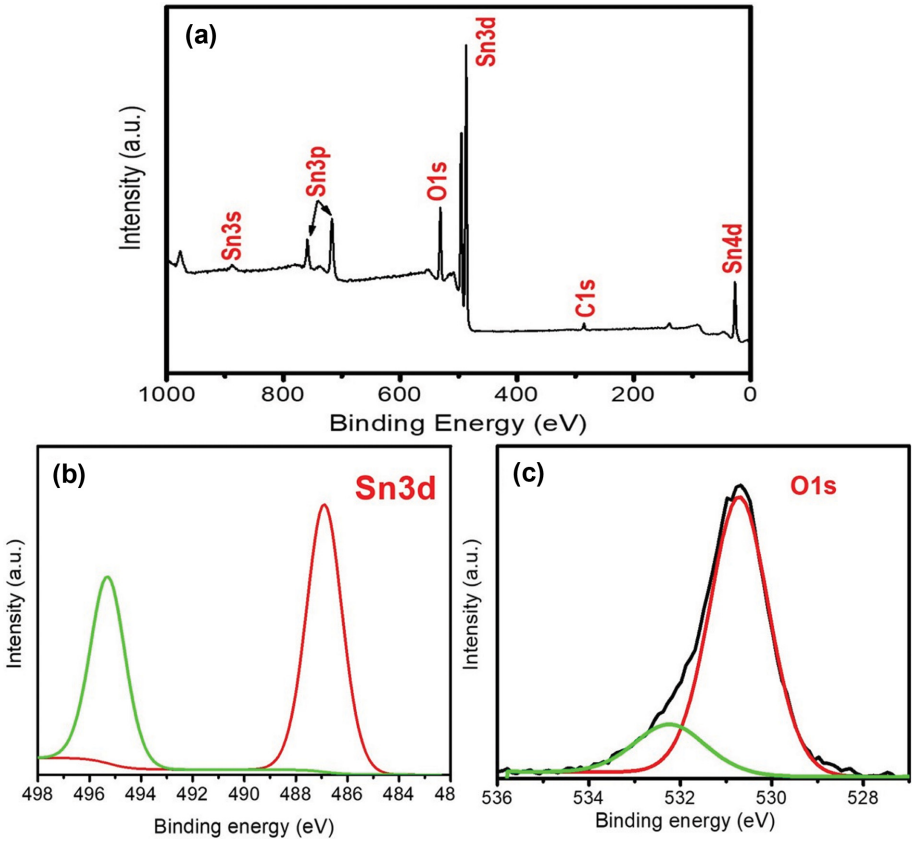


Fig. 10. XPS spectra of SnO_2 nanoparticles from 0.1 M Na_2-EDTA at the optimum leaching conditions using sodium hydroxide: (a) General XPS spectrum; (b) Sn 3d XPS spectrum; (c) O 1s XPS spectra of SnO_2.

nanoparticles [62]. The intense peak located at 621 cm^{-1} interrelated to the Sn-O-Sn vibrations assures the crystallinity of SnO_2 [56]. Many metal oxides having multiple oxygen atoms bound to a metal atom show peak at about 970-1,070 cm^{-1} and this explains the peak at 1,069 cm^{-1} [56]. The absorptions in the range of 3,412-1,628 cm^{-1} designate the O-H group stretching and bending vibrations from H_2O molecules.

The bandgap energy value (E_g) for SnO_2 nanoparticles was predictable from the optical absorption spectra, Fig. 9(b), utilizing the Kubelka-Munk equation [63]:

$$[h\nu F(R\infty)]^2 = B\,(h\nu - E_g) \quad (15)$$

where $F(R\infty)$, $h\nu$, B, and E_g are the Kubelka-Munk function, the energy of the fallen photon, a constant, and the bandgap energy, respectively. The E_g value for SnO_2 NPs was found equal to 2.33 eV, and as seen from the inset figure, SnO_2 has a good light absorption in the ultraviolet region (300-400 nm).

The Sn and O elements, compositions phase, and chemical state were analyzed via XPS. The existence of Sn and O elements is confirmed in the XPS results as shown in Fig. 10(a). The Sn $3d_{3/2}$ and Sn $3d_{5/2}$ peaks shown in Fig. 10(b) might be convoluted into two peaks at 486.9 and 495.8 eV corresponding to SnO_2 rutile-type [64]. The deconvoluted $O1_s$ spectrum validates binding energies of 530.71 and 532.2 eV for two forms of oxygen as shown in Fig. 10(c), which are correlated with SnO_2 [65], verifying the purity of the SnO_2 nanoparticles.

Based on the current study, the process appears promising and eco-friendly compared to conventional techniques. It can be scaled up for synthesizing nanoparticles from Waste PCBs. A comparison of our work with earlier studies for recovering tin as nanoparticles from Waste PCBs is in Table 2.

4. The Degradation of MB

Photocatalytic activity of SnO_2 was assessed by considering the breakdown of MB illuminated by UV light as revealed in Fig. 11(a). The addition of SnO_2 NPs to the dye solution initiated a decrease in the intensity of the absorption peak (at 665 nm) as irradiation time was increased [66]. A 90.0% degradation of MB was achieved after being exposed to UV light for 180 min (Fig. S2 in the supplemental file shows a plot of C_t/C_0 in the degradation of MB).

5. Recyclability of the Photocatalyst

Fig. 11(b) shows the recyclability results revealing that the catalysts can be reused effectively five times with minor changes in degradation percentage from 90% at the first cycle to 83% after the fifth reuse cycle. The process begins with the adsorption of MB molecules on the surface of the photocatalyst, due to the difference in charges between the NP's (negative charges) and the MB molecules (positive charges). Photocatalytic degradation begins when the photocatalyst is irradiated with UV light. The stability and recyclability of SnO_2 nanoparticles were investigated for MB dye degradation in several sequential cycles. After each cycle, the SnO_2 nanoparticles were separated from the reaction mixture by centrifugation and then washed many times with ultrapure water

Table 2. Comparison of different studies carried out for Sn recovery as SnO_2 nanoparticles from waste printed circuit boards

Method	Conditions	Leaching efficiency (%)	Product & morphology	Advantage	Disadvantage	Reference
Chelation Technology	Leaching in 0.1 M Na_2-EDTA at pH: 5 and temperature of 80 °C for 3 h then precipitating SnO_2 by NaOH	99.55	Spherical SnO_2	Simple and ecofriendly	--	Current work
Alkaline pressure oxidation leaching-purification-electrowinning process	Leaching in 2.5 mol/L NaOH for 3 h with stirring at 150 °C, oxygen partial pressure of 2.0 MPa and solid to liquid ratio of 1 : 4	98.2	Sn (uniform flake structure)	- Low energy consumption - Low capital investment	Multi step operation	[70]
Thermal transformation	PCBs sample was treated in a horizontal tube furnace at 900 °C for 30 min under argon atmosphere at atmospheric pressure	*NR	Cu-Sn (Spherical particle)	- Simple operation	- High energy consumption - High capital investment Production of gases	[71]
Combination of leaching, electrochemical ion exchange and electrodeposition	Scrap PCBs were dissolved in 4 M HNO_3 where tin formed a precipitate (meta stannic acid), this precipitate then dissolved in 1.5 M HCl. Tin was electrodeposited from this solution	>95	Sn	- Simple and efficient separation method	- Use of corrosive acids	[30]
Leaching with assistance of ultrasound and Microwaves	Crushed WPCBs were leached with 7.0 M HNO_3 solution for 2 h at 60 °C. SnO_2 precipitation by solution evaporation by heating at 85 °C for 6 h, with ultrasound irradiation for 1 h, and microwave irradiation for 15 min	*NR	SnO_2-Ag (Spherical shape)	High purity particles	- Use of corrosive acids - High energy consumption - High capital investment -	[72]

*NR: Not reported by authors.

and dried at room temperature. In the next cycle, the SnO_2 nanoparticles were reused for the degradation of fresh dye solution.

A plausible mechanism for the MB photocatalytic break down by SnO_2 NPs is that an exciton is generated when irradiating a catalyst surface with energy whose bandgap is larger than that of the catalyst. This exciton forms a hole (h+) and an electron (e−) in the valence and conduction bands of the SnO_2 NPs. The h+ and the e− will serve as oxidants to oxidize the dye and a reductant reduces oxygen on the SnO_2 giving colorless degradation byproducts (CO_2 and H_2O) [67,68] as proposed in Fig. 11(c) and the photocatalysis route and products of MB degradation are suggested to occur as shown in Fig. 12 [69].

The current work exhibits excellent photocatalytic activity for waste-derived SnO_2 nanoparticles with reasonable irradiation time when compared to other existing photocatalysts prepared from pure chemicals. This comparison (shown in Table S2 in the supplemental file) clarifies that these prepared SnO_2 NPs are considered good photocatalysts like other catalysts previously reported in the literature.

CONCLUSIONS

To achieve the best parameters for tin retrieval from the WPCBs, comparative leaching studies were performed using Na_2-EDTA chelating agent and two conventional inorganic oxidizing acids. Na_2-EDTA was found to be an excellent lixiviant to extract tin selectively in comparison to HNO_3 and H_2SO_4 acids. Leaching of tin metal reached 99.55% using 0.1 M Na_2-EDTA at a liquid/solid ratio of 30, temperature 80 °C, and mixing time 3 hours. The leaching kinetics of tin in Na_2-EDTA was found following the diffusion through the liquid film model with activation energy, E_a=15.2 $kJmol^{-1}$. From the leach liquor, irregularly spherical SnO_2 NPs with average size 8-12 nm were prepared using NaOH at pH 9.0. The prepared SnO_2 NPs showed a reasonable photocatalytic degradation (90%) for MB solution after 180 minutes (3 hours) of UV illumination. The reusability of the catalyst nanoparticles was tested for five consecutive cycles and showed good reusability with a minor decrease (7%) after the fifth cycle. The presented method here can be looked at as a new and eco-friendly technique for tin recovery

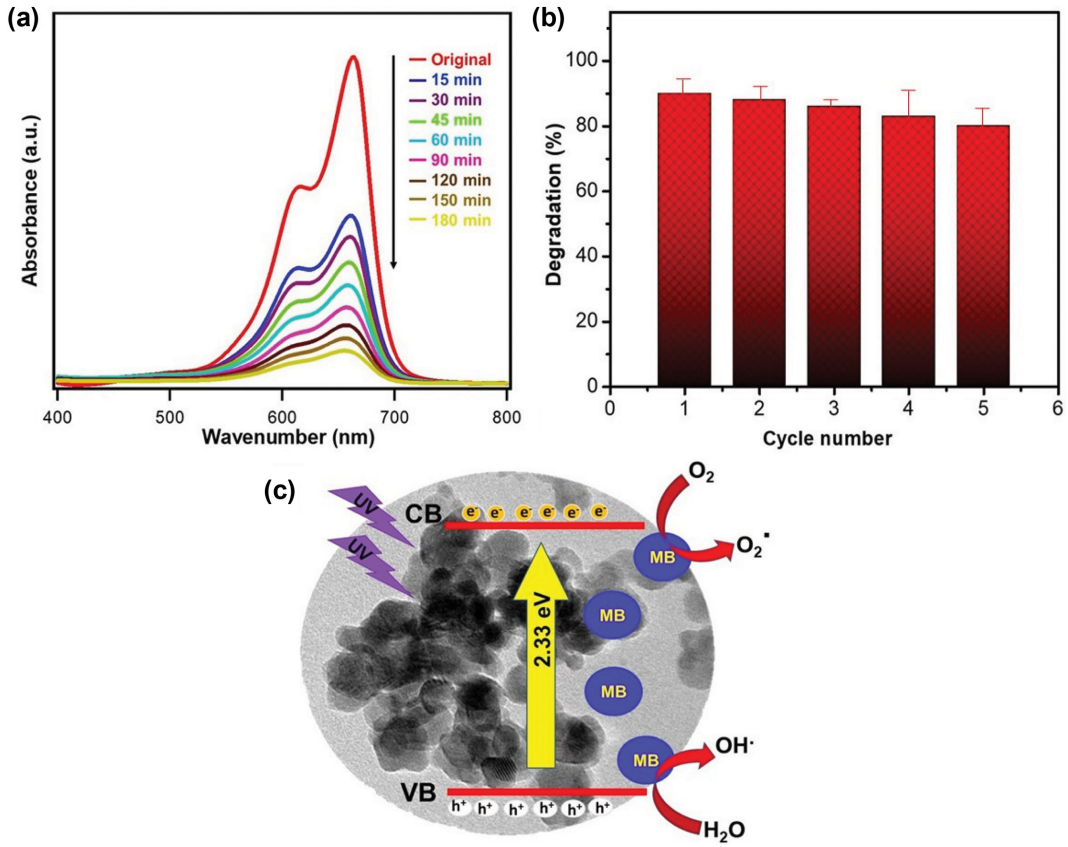


Fig. 11. (a) Time-contingent UV-vis spectra of MB breakdown by SnO_2 nanoparticles, (b) recycling experiment of SnO_2 samples on the photodegradation MB, (c) proposed mechanism of the degradation of MB dye by SnO_2 nanoparticles under UV light.

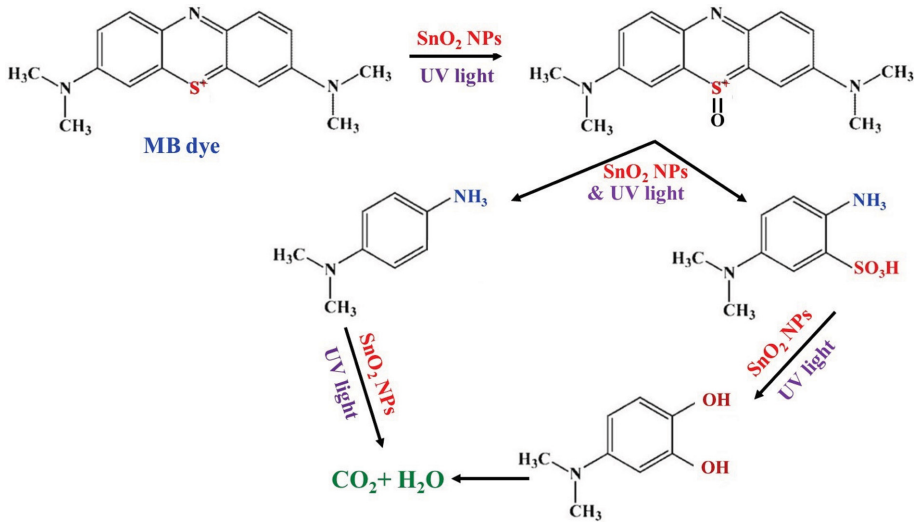


Fig. 12. Photocatalytic degradation route and products of MB dye by SnO_2 nanoparticles.

as SnO_2 NPs that can be applied as an efficacious photocatalyst for dye degradation.

CONFLICT OF INTEREST

No conflict of interest to declare.

ACKNOWLEDGEMENT

The authors appreciatively acknowledge the funding offered by the Science, Technology and Innovation Funding Authority (STIFA), Egypt, for this research under project No. 29001.

SUPPORTING INFORMATION

Additional information as noted in the text. This information is available via the Internet at http://www.springer.com/chemistry/journal/11814.

REFERENCES

1. S. M. Abdelbasir, S. S. M. Hassan, A. H. Kamel and R. S. El-Nasr, *Environ. Sci. Pollut. Res.*, **25**, 16533 (2018).
2. Y. Zhou, W. Wu and K. Qiu, *Waste Manag.*, **30**, 11 (2010).
3. S. M. Abdelbasir, C. T. El-Sheltawy and D. M. Abdo, *J. Sustain. Metall.*, **4**, 295 (2018).
4. R. M. Shalaby, *J. Alloys Compd.*, **505**, 113 (2010).
5. S. Arya and S. Kumar, *Bioengineered*, **11**, 640 (2020).
6. B. H. Robinson, *Sci. Total Environ.*, **408**, 183 (2009).
7. X. Zeng, J. Li, H. Xie and L. Liu, *Chemosphere*, **93**, 1288 (2013).
8. S. Ilyas, R. R. Srivastava and H. Kim, *J. Hazard. Mater.*, **416**, 125769 (2021).
9. J. M. Yoo, J. Jeong, K. Yoo, J. C. Lee and W. Kim, *Waste Manag.*, **29**, 1132 (2009).
10. J. C. Lee, H. T. Song and J. M. Yoo, *Resour. Conserv. Recycl.*, **50**, 380 (2007).
11. H. T. Fan, J. Li, M. M. Guo, X. L. Fan, D. S. Zhang, Z. J. Su and J. Wang, *Desalin. Water Treat.*, **50**, 51 (2012).
12. H. B. Xu, H. T. Fan, X. J. Jiang and T. Sun, *Asian J. Chem.*, **23**, 3827 (2011).
13. Ž. Kamberović, M. Ranitović, M. Korać, Z. Andjić, N. Gajić, J. Djokić and S. Jevtić, *Metals*, **8**, 6 (2008).
14. F. Xiu, H. Weng, Y. Qi, G. Yu, Z. Zhang, F. Zhang and M. Chen, *Waste Manag.*, 60 (2017).
15. R. Seif El-Nasr, S. M. Abdelbasir, A. H. Kamel and S. S. M. Hassan, *Sep. Purif. Technol.*, **230**, 115860 (2020).
16. Y. J. Park and D. J. Fray, *J. Hazard. Mater.*, **164**, 1152 (2009).
17. S. Arya, A. Patel, S. Kumar and S. H. O. W. Pau-Loke, *Environ. Pollut.*, In Press, 117033 (2021).
18. I. Janakova, E. Pertile, P. Fecko, I. Janakova, E. Pertile and E. Kulova, *Metallurgia*, **50**, 1 (2011).
19. C. Q. Cheng, F. Yang, J. Zhao, L. H. Wang and X. G. Li, *Corros. Sci.*, **53**, 1738 (2011).
20. M. K. Jha, A. Kumari, P. K. Choubey, J. C. Lee, V. Kumar and J. Jeong, *Hydrometallurgy*, **121-124** (2012).
21. T. Havlik, D. Orac, M. Petranikova and A. Miskufova, *Waste Manag.*, **31**, 1542 (2011).
22. H.-S. Hong, H.-C. Jung, G.-H. Kim and M.-S. Kong, *J. Korean Powder Metall. Inst.*, **16**, 351 (2009).
23. C. Yang, Q. Tan, L. Liu, Q. Dong and J. Li, *ACS Sustain. Chem. Eng.*, **5**, 9586 (2017).
24. S. Virolainen, D. Ibana and E. Paatero, *Hydrometallurgy*, **107**, 56 (2011).
25. G.-H. Kim, H.-S. Hong and H.-C. Jung, *J. Korean Powder Metall. Inst.*, **19**, 405 (2012).
26. T. Havlik, D. Orac, M. Petranikova, A. Miskufova, F. Kukurugya and Z. Takacova, *J. Hazard. Mater.*, **183**, 866 (2010).
27. X. Zhang, J. Guan, Y. Guo, X. Yan, H. Yuan, J. Xu, J. Guo, Y. Zhou, R. Su and Z. Guo, *ACS Sustain. Chem. Eng.*, **3**, 1696 (2015).
28. S. K. Kim, J. C. Lee ande K. Yoo, *Hydrometallurgy*, **165**, 143 (2016).
29. S. Gu, B. Fu, G. Dodbiba, T. Fujita and B. Fang, *RSC Adv.*, **7**, 52017 (2017).
30. A. Mecucci and K. Scott, *J. Chem. Technol. Biotechnol.*, **77**, 449 (2002).
31. S. Tazikeh, A. Akbari, A. Talebi and E. Talebi, *Mater. Sci. Pol.*, **32**, 98 (2014).
32. L. Man, J. Zhang, J. Wang, H. Xu and B. Cao, *Particuology*, **11**, 242 (2013).
33. G. E. Patil, D. D. Kajale, V. B. Gaikwad and G. H. Jain, *Int. Nano Lett.*, **2**, 17 (2012).
34. H. Ullah, I. Khan, Z. H. Yamani and A. Qurashi, *Ultrason. Sonochem.*, **34**, 484 (2017).
35. L. M. Cukrov, P. G. McCormick, K. Galatsis and W. Wlodarski, *Sensors Actuators, B Chem.*, **77**, 491 (2001).
36. F. Davar, M. Salavati-Niasari and Z. Fereshteh, *J. Alloys Compd.*, **496**, 638 (2010).
37. J. Ba, J. Polleux, M. Antonietti and M. Niederberger, *Adv. Mater.*, **17**, 2509 (2005).
38. C. H. Shek, J. K. L. Lai and G. M. Lin, *Nanostructured Mater.*, **11**, 887 (1999).
39. D. Yu, D. Wang, W. Yu and Y. Qian, *Mater. Lett.*, **58**, 84 (2004).
40. B. Teldja, B. Noureddine, B. Azzeddine and T. Meriem, *Optik (Stuttg)*, **209**, 164586 (2020).
41. H. Wang, F. Fu, F. Zhang, H. E. Wang, S. V. Kershaw, J. Xu, S. G. Sun and A. L. Rogach, *J. Mater. Chem.*, **22**, 2140 (2012).
42. W. Tian, C. Zhang, T. Zhai, S. L. Li, X. Wang, M. Liao, K. Tsukagoshi, D. Golberg and Y. Bando, *Chem. Commun.*, **49**, 3739 (2013).
43. S. Xu, D. Li, J. Guo, Y. Hu and P. Yang, *J. Phys. Chem. Solids*, **148**, 109763 (2021).
44. N. Tammanoon, A. Wisitsoraat, A. Tuantranont and C. Liewhiran, *J. Alloys Compd.*, **871**, 159547 (2021).
45. R. K. Nekouei, F. Pahlevani, M. Mayyas, S. Maroufi and V. Sahajwalla, *J. Environ. Chem. Eng.*, **7**, 103133 (2019).
46. A. Shawky, S. M. El-Sheikh, M. N. Rashed, S. M. Abdo and T. I. El-Dosoqy, *J. Environ. Chem. Eng.*, **7**, 103174 (2019).
47. S. M. Abdelbasir, A. M. Elseman, F. A. Harraz, Y. M. Z. Ahmed, S. M. El-Sheikh and M. M. Rashad, *New J. Chem.*, **45**, 6 (2021).
48. S. K. Tammina, B. K. Mandal and N. K. Kadiyala, *Environ. Nanotechnology, Monit. Manag.*, **10**, 339 (2018).
49. M. M. Khan, S. F. Adil and A. Al-Mayouf, *J. Saudi Chem. Soc.*, **19**, 462 (2015).
50. S. P. Kim, M. Y. Choi and H. C. Choi, *Mater. Res. Bull.*, **74**, 85 (2016).
51. V. H. Ha, J. C. Lee, T. H. Huynh, J. Jeong and B. D. Pandey, *Hydrometallurgy*, **149**, 118 (2014).
52. C. Kim, Y. Lee and S. K. Ong, *Chemosphere*, **51**, 845 (2003).
53. M. Souada, C. Louage, J. Y. Doisy, L. Meunier, A. Benderrag, B. Ouddane, S. Bellayer, N. Nuns, M. Traisnel and U. Maschke, *Ultrason. Sonochem.*, **40**, 929 (2018).
54. S. Ghosh and S. Roy, *J. Sol-Gel Sci. Technol.*, **81**, 769 (2017).
55. K. Yoo, J. C. Lee, K. S. Lee, B. S. Kim, M. S. Kim, S. K. Kim and B. D. Pandey, *Mater. Trans.*, **53**, 2175 (2012).
56. T. A. Dontsova, S. V. Nagirnyak, V. V. Zhorov and Y. V. Yasiievych, *Nanoscale Res. Lett.*, **12**, 332 (2017).
57. G. Chauhan, K. K. Pant and K. D. P. Nigam, *Environ. Sci. Process. Impacts*, **17**, 12 (2015).

58. S. Goel, K. K. Pant and K. D. P. Nigam, *J. Hazard. Mater.*, **171**, 253 (2009).
59. G. Chauhan, K. K. Pant and K. D. P. Nigam, *Ind. Eng. Chem. Res.*, **52**, 16724 (2013).
60. D. Fangueiro, A. Bermond, E. Santos, H. Carapuça and A. Duarte, *Anal. Chim. Acta*, **459**, 245 (2002).
61. R. C. Abruzzi, B. A. Dedavid and M. J. R. Pires, *Ceramica*, **61**, 328 (2015).
62. L. Hauser, S. Tandy, R. Schulin and B. Nowack, *Environ. Sci. Technol.*, **39**, 6819 (2005).
63. S. M. Abdelbasir, S. M. El-Sheikh, M. M. Rashad and D. A. Rayan, *Electron. Mater. Lett.*, **14**, 505 (2018).
64. W. Xia, H. Wang, X. Zeng, J. Han, J. Zhu, M. Zhou and S. Wu, *CrystEngComm*, **16**, 6841 (2014).
65. S. Das, D. Y. Kim, C. M. Choi and Y. B. Hahn, *J. Cryst. Growth*, **314**, 171 (2011).
66. A. Diallo, E. Manikandan, V. Rajendran and M. Maaza, *J. Alloys Compd.*, **681**, 561 (2016).
67. J. Osuntokun, D. C. Onwudiwe and E. E. Ebenso, *J. Clust. Sci.*, **28**, 1883 (2017).
68. S. Suthakaran, S. Dhanapandian, N. Krishnakumar and N. Ponpandian, *Mater. Res. Express*, **6**, 0850i3 (2019).
69. S. T. T. Le, W. Khanitchaidecha and A. Nakaruk, *Bull. Mater. Sci.*, **39**, 569 (2016).
70. T. Yang, P. Zhu, W. Liu, L. Chen and D. Zhang, *Waste Manag.*, **68**, 449 (2017).
71. A. Shokri, F. Pahlevani, K. Levick, I. Cole and V. Sahajwalla, *J. Clean. Prod.*, **142**, 2586 (2017).
72. P. Cerchier, M. Dabalà and K. Brunelli, *JOM*, **69**, 1583 (2017).

Supporting Information

Recovery of Tin as Tin oxide nanoparticles from waste printed circuit boards for photocatalytic dye degradation

Dina Magdy Abdo*, Sabah Mohamed Abdelbasir*,†, Shakinaz Taha El-Sheltawy, and Ibrahim Ahmed Ibrahim***

*Central Metallurgical Research and Development Institute, P.O. Box: 87, Helwan, 11421, Cairo, Egypt
**Faculty of Engineering, Cairo University, Giza, Egypt
(*Received 16 February 2021 • Revised 1 May 2021 • Accepted 4 May 2021*)

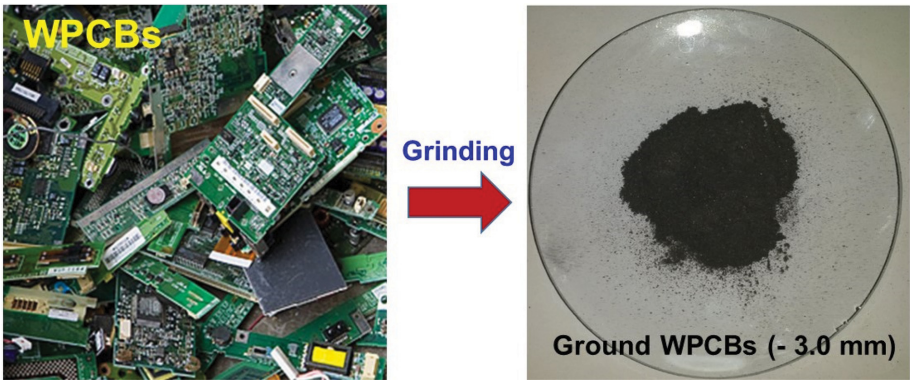


Fig. S1. A photo of the used WPCBs sample before and after grinding.

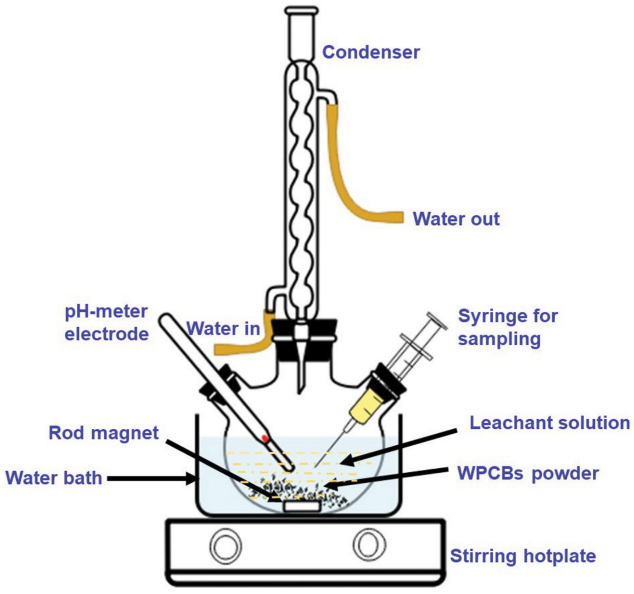


Fig. S2. A sketching of the used WPCBs leaching system.

Table S1. Apparent rate constants (k_1, k_r, k_d and k_m) for the kinetic models and correlation coefficients

Parameter	Diffusion through the liquid film		Surface chemical reaction		Diffusion through the product layer		Mixed kinetic model	
	X		$1-(1-x)^{1/3}$		$1-3(1-x)^{2/3}+2(1-X)$		$(1-(1-x)^{1/3})^2$	
T (°C)	k (min^{-1})	R^2	k (min^{-1})	R^2	k (min^{-1})	R^2	k (min^{-1})	R^2
50	0.1715	0.94	0.2281	0.93	0.2676	0.94	0. 25301	0.89
70	0.1005	0.96	0.1333	0.90	0.1805	0.90	0.1395	0.85
80	0.0992	0.97	0.1948	0.94	0.2396	0.95	0.2436	0.94
90	0.0818	0.96	0.1979	0.95	0.2266	0.94	0.26601	0.93

Table S2. Comparison of performance characteristics of SnO_2 photocatalysts for the degradation of MB pollutant

Nanoparticles	Dye	Illumination light	Illumination time (min)	Degradation (%)	References
SnO_2	MB	UV	180	90	Current work
SnO_2	MB	UV	120	90	[1]
SnO_2/SnO	MB	UV	180	90.28	[2]
SnO_2	MB	UV	30	90	[3]
SnO_2	MB	UV	180	79	[4]
SnO_2	MB	UV	120	90	[5]
SnO_2	*CR	UV	97	100	[6]
SnO_2	**MO	UV	180	100	[7]

*CR: Congo Red, **MO: Methyl orange.

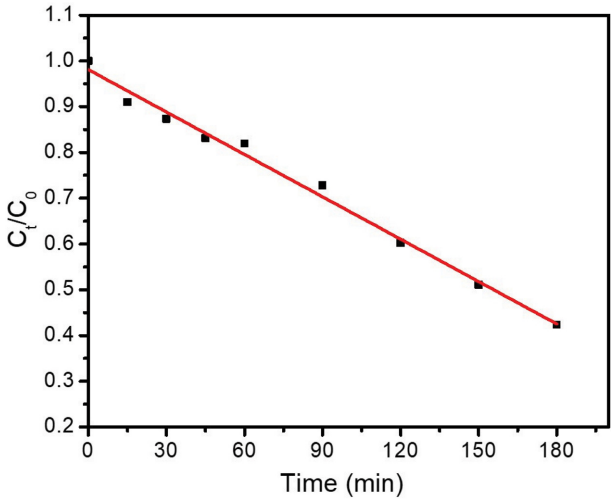


Fig. S3. Photocatalytic degradation of MB over SnO_2 nanoparticles with illumination time.

REFERENCES

1. M. Vatanparast and M. T. Taghizadeh, *J. Mater. Sci. Mater. Electron.*, **27**, 54 (2016).
2. K. Santhi, C. Rani and S. Karuppuchamy, *J. Alloys Compd.*, **662**, 102 (2016).
3. S. K. Tammina, B. K. Mandal and N. K. Kadiyala, *Environ. Nanotechnology, Monit. Manag.*, **10**, 339 (2018).
4. S. P. Kim, M. Y. Choi and H. C. Choi, *Mater. Res. Bull.*, **74**, 85 (2016).
5. P. Van Viet, C. M. Thi and L. Van Hieu, *J. Nanomater.*, **2016**, 1 (2016).
6. C. M. Ma, G. B. Hong and S. C. Lee, *Catalysts*, **10**, 792 (2020).
7. N. John, N. J. Tharayil and M. Somaraj, *J. Mater. Sci. Mater. Electron.*, **28**, 5860 (2017).